ADVANCED FUNCTIONAL MATERIALS
www.afm-journal.de

Enhancing Performance Stability of Electrochemically Active Polymers by Vapor-Deposited Organic Networks

Xianwen Mao, Andong Liu, Wenda Tian, Xiaoxue Wang, Karen K. Gleason, and T. Alan Hatton**

Performance stability of electrochemically active polymers (EAPs) remains one of the greatest and long-standing challenges with regard to EAP-based technologies for a myriad of energy, biomedical, and environmental applications. The performance instability of EAPs originates from their structural alteration under repeated charge–discharge cycling and/or flexing. In this work, a conceptually new "soft confinement" strategy to enhance EAP performance stability, including cyclic and mechanical, by using rationally designed, vapor-deposited organic networks is presented. These chemically cross-linked networks, when in contact with an electrolyte solution, turn into ultrathin, elastic hydrogel coatings that encapsulate conformally the EAP micro-/nanostructures. Such hydrogel coatings allow easy passage of ions that intercalate with EAPs, while simultaneously mitigating the structural pulverization of the EAPs and/or their detachment from substrates. Fundamentally distinct from extensively studied "scaffolding" or "synthetic" approaches to stabilizing EAPs, this soft confinement strategy relies on a postmodification step completely decoupled from the EAP synthesis/fabrication, and enjoys the unique advantage of substrate-independency. Hence, this strategy is broadly applicable to various types of EAPs. The proposed stability enhancement strategy is demonstrated to be effective for a range of EAP systems with differing chemical and morphological characteristics under various testing conditions (repeated charging/discharging, bending, and twisting).

1. Introduction

The growing research interest in electrochemically active polymers (EAPs) stems from their key roles in diverse applications, such as energy storage and conversion,[1–4] drug delivery and monitoring,[5,6] organic (bio)electronics development,[7,8] neural interface engineering,[9,10] and chemical and environmental separations.[11–13] Performance stability remains one of the greatest and long-standing challenges with regard to EAP-based technologies, particularly with prolonged charge/discharge cycling and/or the application of mechanical stresses. Enhanced stability would enable practical long-term operation, as well as meet the increasing demand for flexible electronic devices.[14–16] Possible mechanisms causing the cycling instability of EAPs include structural pulverization due to repeated swelling and shrinkage of polymer backbones, and collapse of initially present ion channels resulting in difficulty of subsequent redoping.[14,17–20] A widely adopted approach to enhancing EAP stability is integration of the EAPs with conductive scaffolds, such as porous graphite foams,[21] carbon nanotube sponges,[22] nickel foams,[23] and partially exfoliated graphite.[18] These scaffolds are usually porous and dimensionally stable, and thus act as robust supports for EAP films to reduce their structural alteration. Such a "scaffolding" approach relies on effective hybridization of the EAP with the underlying conductive substrate, a nontrivial task. The integration process often requires judicious surface modification of the scaffold materials to create specific interactions (e.g., covalent bonding, π–π stacking) with the EAP, and a lengthy screening process to determine the reaction conditions for the growth of a certain EAP on the scaffold. A few less common methods based on deliberate synthetic strategies for improving EAP stability have also been demonstrated, such as creation of supramolecular structures,[24] synthesis of hyperbranched EAPs,[25] and dopant/EAP engineering.[26,27] These scaffolding and synthetic approaches have shown great promise when applied to certain types of EAP systems, but are highly dependent on the chemical nature of the EAP. Hence, an optimized reaction condition usually applies to only one specific EAP. In addition, morphology control of the EAP is not decoupled from the integration or synthesis process: the scaffolding or synthetic approach that results in enhanced stability could also yield an undesired morphology with compromised electrochemical properties (e.g., lower energy density, lower sensitivity, and diminished functionalities).

Here, we report a conceptually new strategy to enhance EAP performance stability using a rationally designed polymer network that provides "soft confinement" for an EAP system. We hypothesize that an EAP system, whose microstructure is confined conformally by an ultrathin elastic polymer network, would exhibit improved morphological integrity, leading to low extents of structural pulverization and ion channel collapse. In contrast to the scaffolding and synthetic approaches studied

Dr. X. Mao, Dr. A. Liu, W. Tian, X. Wang, Prof. K. K. Gleason, Prof. T. Alan Hatton
Department of Chemical Engineering
Massachusetts Institute of Technology
77 Massachusetts Avenue, Cambridge, MA 02139, USA
E-mail: kkg@mit.edu; tahatton@mit.edu
DOI: 10.1002/adfm.201706028

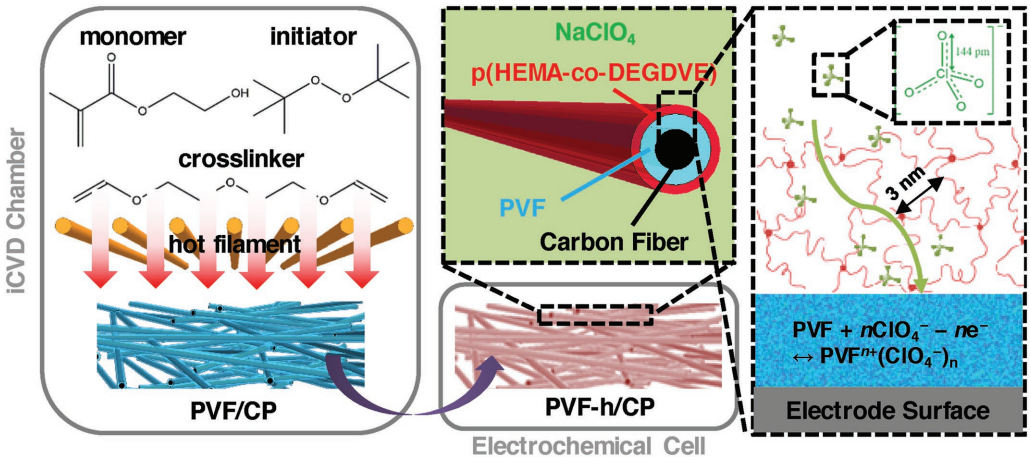

Figure 1. Schematic illustration of the "soft confinement" concept. An iCVD-synthesized polymer network is deposited conformally on EAP microstructures. Here, P(HEMA-*co*-DEGDVE) (or PHEMAx) and PVF were used as the model polymer network and EAP, respectively.

extensively in the past,[18,21–27] our soft confinement approach is applicable independently of the surface chemistry and morphology of the EAPs to be stabilized, and hence can be used flexibly in various types of EAP systems with different structures for a range of applications. The concept of soft confinement is illustrated schematically in **Figure 1**. To achieve effective stability enhancement without compromising the desired electrochemical functionalities of EAPs, the material system offering the soft confinement should be able to (i) completely and conformally coat the interfaces of micro-/nanostructured EAPs without blocking the structures/pores, (ii) tolerate the volumetric alteration of EAPs without being mechanically degraded itself, and (iii) allow easy passage of electrolyte ions for subsequent doping/dedoping of the inner EAPs. In this work, we designed a hydrogel coating that meets all the preceding requirements for soft confinement. Such a hydrogel coating was formed in an aqueous electrolyte by the swelling of a polymer network synthesized via a nondestructive gas-phase process, initiated chemical vapor deposition (iCVD).

Our approach to enhancing EAP stability exhibits many advantages. First, the coating process using iCVD does not rely on the surface energy of the EAP. Nor does it depend on the surface chemistries of, or specific interactions with, the EAP, and thus is broadly applicable to EAPs of various chemical natures. It should be noted that our study focuses on electrochemically active polymeric systems, i.e., excluding other systems whereby electrochemical driving forces are absent, such as dielectric electroactive polymers for actuator applications.[28] Furthermore, our polymer coating and the resulting hydrogel thin film conform to a structured interface and therefore are applicable to highly porous, nanostructured EAP systems, which are of enormous significance for various electrochemical applications. This is because iCVD allows the conformal modification of pores with diameters down to sub-100 nm, with exquisite control of the coating thickness.[29,30] Additionally, the coating process using vapor phase precursors is solvent-free, thus avoiding common issues associated with solution-based modifications such as polymer leaching and deformation. It is also worth mentioning that iCVD, fundamentally different from high-temperature CVD, is thermally nondestructive and therefore can be applied to modify a fabricated EAP electrode in situ. Finally, yet importantly, the iCVD technique has proven scalability for potential commercialization; large-area batch (>1 m diameter) and roll-to-roll systems have been utilized for manufacturing.[31]

2. Results and Discussion

The prototype polymer network developed in our study to coat and stabilize EAPs is poly(2-hydroxyethyl methacrylate) (PHEMA) cross-linked by di(ethylene glycol) divinyl ether (DEGDVE). The chemical cross-linking was deliberately introduced to enhance the structural stability of the resulting iCVD hydrogel.[32] Hereafter, the cross-linked PHEMA is denoted PHEMAx. As the first proof of concept, we studied the effects of the hydrogel coating on the electrochemical cyclic stability of a model EAP, polyvinylferrocene (PVF), which has various important electrochemical applications such as energy storage,[33] biosensing,[34,35] and redox-tunable catalysis[36] and separation.[11,12] Prior to the iCVD treatment, PVF was deposited potentiostatically on a conductive carbon paper (CP) substrate to generate a PVF/CP hybrid, which was subsequently transferred into an iCVD chamber for conformal coating of PHEMAx throughout the porous PVF/CP electrodes. Hereafter, the nomenclature "A/B" or "A-h/B" is used to identify a multicomponent construct, where "A" indicates the active material system (e.g., an EAP), "A-h" indicates A is modified with a PHEMAx coating that turns into a hydrogel upon contact with water, and "B" is the conductive substrate upon which A is deposited. The resulting PVF-h/CP system consisted of ternary core–shell fibers with individual components from the innermost being carbon fiber, PVF, and PHEMAx. PHEMAx was selected as the polymer matrix for the soft confinement layer because of its ability to form a hydrogel upon swelling in aqueous electrolytes, allowing the transport of ions.[32,37] The ultrathin hydrogel outermost layer, whose properties can be controlled precisely by iCVD, should not add a substantial resistance to the ion

transport. More importantly, iCVD PHEMAx-based hydrogels generally exhibit moderate swelling ratios (<1.55),[32] which is crucial for our soft confinement concept; high water content would compromise the gel's mechanical strength, whereas low water content would result in small mesh sizes and therefore high resistance to ion transport. The PHEMAx coating synthesized under our conditions had a swelling ratio of 1.40 ± 0.04, corresponding to a mesh size of 3.12 ± 0.66 nm based on the Flory–Huggins theory, assuming uniaxial swelling of an elastic network (Section S2, Supporting Information).[37] Such a mesh size would allow easy transport of most aqueous electrolyte ions for energy storage applications (Table S1, Supporting Information); perchlorate and sulfate ions used in our study have hydrated ion sizes of 0.34 and 0.38 nm, respectively.[38] The Fourier transform infrared spectrum of PHEMAx confirms the retention of HEMA functional groups during iCVD synthesis (Figure S1a, Supporting Information). The water contact angle of a PHEMAx film on a smooth silicon wafer was measured to be 20.70° ± 0.12° (Figure S1b, Supporting Information), demonstrating the hydrophilicity of PHEMAx.

Scanning electron microscopic (SEM) imaging of CP, PVF/CP, and PVF-h/CP (**Figure 2**a–c, respectively) shows clear morphological differences across the three systems. Compared to bare CP, PVF/CP exhibits a larger fiber diameter and a rougher surface, indicating the presence of the PVF polymer. After being coated with PHEMAx, the fiber displays a further increase in diameter and a smoother surface, revealing a conformal PHEMAx layer wrapping around the PVF/CP fibers. X-ray photoelectron spectroscopic (XPS) survey scans of CP, PVF/CP, and PVF-h/CP are displayed in Figure 2d. PVF/CP shows pronounced $Fe_{2p1/2}$ and $Fe_{2p3/2}$ peaks at 715 and 705 eV, respectively, characteristic of ferrocene, while these peaks are completely absent for PVF-h/CP. This suggests that, after the iCVD treatment, the surface of the PVF/CP network was fully covered by PHEMAx. Notably, PVF-h/CP has an O/C ratio of 0.52 ± 0.06, consistent with the theoretical value (0.5) for HEMA, corroborating that the outermost shell in PVF-h/CP consists mainly of PHEMA.

Next, we performed electrochemical tests on PVF-h/CP. For details on all electrochemical measurements, see Section S5 (Supporting Information). Throughout this report, the current density (A g^{-1}) and specific capacity (C g^{-1}) of a electrode system are reported with respect to the total mass of the polymer components, including both the EAP and the PHEMAx coating (if any), unless otherwise noted. Electrochemical cycling stability of PVF-h/CP was first examined using cyclic voltammetry (CV). As shown in Figure 2e, PVF/CP, without iCVD treatment, exhibits a significantly reduced specific capacity after 15 000 cycles (only ≈12% retention), while PVF-h/CP with 1.5–4.5 h iCVD treatments shows virtually 100% capacity retention. With only 0.5 h iCVD treatment, improved stability relative to unmodified PVF/CP was still observed (≈54% retention after 15 000 cycles). It is imperative that the improved cycling stability not be at the expense of the specific capacities. From CVs obtained at the fifth cycle (i.e., before significant degradation occurred) (Figure 2f), we observed comparable current densities before and after the iCVD treatments, indicating that inclusion of the hydrogel layers did not reduce the specific capacities

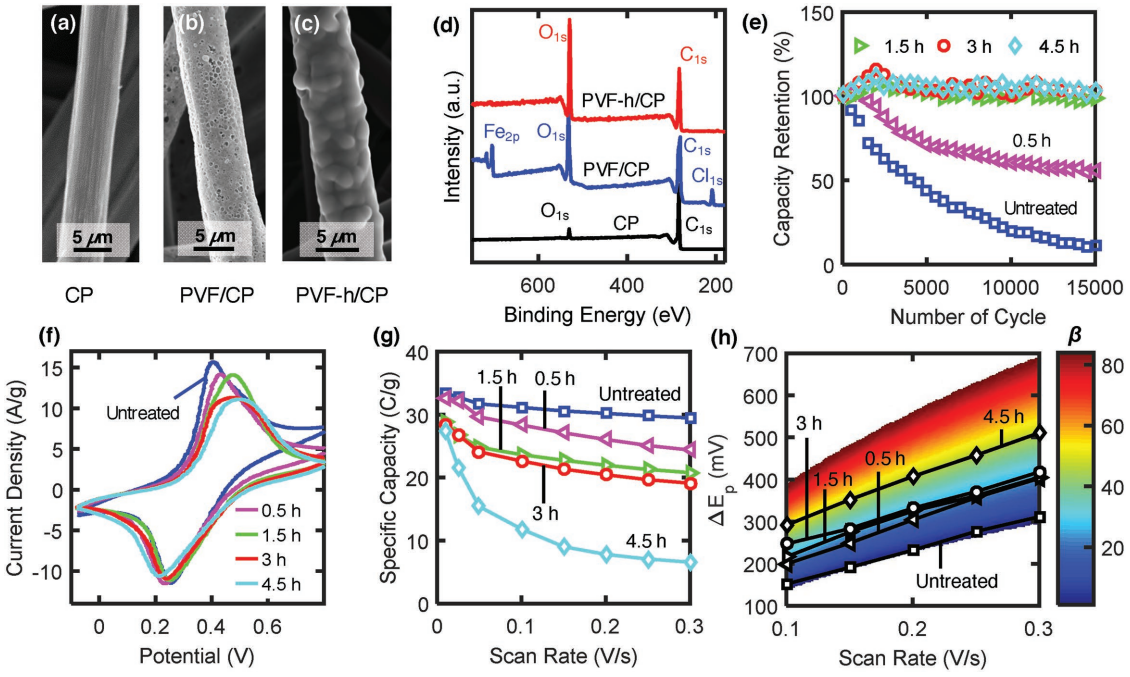

Figure 2. Representative SEM images of a) bare CP, b) PVF/CP, and c) PVF-h/CP (3 h iCVD treatment). d) XPS spectra of bare CP, PVF/CP, and PVF-h/CP (3 h iCVD treatment). e) Capacity retention versus the number of CV cycles, f) CV curves during the fifth cycle, and g) specific capacity versus scan rate for PVF/CP (untreated) and PVF-h/CP with 0.5, 1.5, 3, and 4.5 h iCVD treatments. CV was performed at 0.1 V s^{-1} in 0.5 M $NaClO_4$ using a three-electrode configuration. h) Simulated ΔE_p values versus scan rate with different $\beta = D_{ct}^{PVF}/D_{ct}^{PVF\text{-}h}$ values (heat map), overlaid with the experimentally measured ΔE_p values (black symbols).

significantly. The difference in potential between the anodic and cathodic peaks in CVs (ΔE_p) appears to increase with the iCVD treatment, suggestive of increased ion diffusion resistance, which may affect rate capabilities. To evaluate the rate performance, we plot the specific capacity versus scan rate (Figure 2g), from which it can be seen that with a prolonged iCVD treatment (4.5 h), a markedly jeopardized rate performance resulted. Therefore, 3 h appears to be an optimal iCVD treatment time that yields the best combination of capacity retention and rate performance preservation. We observed slightly reduced specific capacities for the coated samples at low scan rates, because of the added weight of electrochemically inert PHEMAx component. If we normalize to the mass of PVF only, we actually obtain slightly increased specific capacities; for instance, the specific capacities obtained at 0.01 V s^{-1} for PVF/CP and PVF-h/CP with a 3 h iCVD treatment are 33.4 and 35.7 C g^{-1}, respectively. The surface covered by PHEMAx had a higher degree of hydrophilicity (water contact angle = 20.7°) than that covered by ferrocene (water contact angle = 71°);[35] a hydrogel coating on PVF could facilitate its interaction with percholorate.

Having demonstrated the stabilizing effects of the 3 h iCVD PHEMAx, we hypothesize that, mechanistically, the soft confinement coating is able to confine PVF to the vicinity of its conductive networks even when it is pulverized, therefore preserving the capacity of PVF during cyclic operation. To validate this hypothesis, we performed tensile tests on a simulated PHEMAx coating. The PHEMAx hydrogel can elongate ≈109% before it breaks; such a high elongation at break is sufficient to accommodate the volumetric swelling of the PVF film (≈32%) (see Section S3 in the Supporting Information for a detailed discussion).[39]

Further, we elucidated quantitatively the effects of the hydrogel coating on the electrochemical charge transport dynamics in PVF. Mechanistically, charge propagation in an EAP system with discrete redox sites (e.g., PVF) is a diffusive process that relies on sequential electron exchange between adjacent redox groups under restricted local motions of polymer chains.[19,40,41] This diffusive process is usually described by an effective charge transport diffusion coefficient (D_{ct}). The presence of the hydrogel coating would hinder diffusion of the counterion (i.e., perchlorate) from the bulk solution, and, consequently, would affect the charge transport kinetics of the PVF film, leading to lowered D_{ct} values. Notably, the rate of ion intercalation into the polymer film and subsequent binding with ferrocene govern the redox transformation kinetics of PVF. Experimentally, the hindered charge transport dynamics in PVF was manifested by the increased ΔE_p values (Figure 2f). To quantify the effects of iCVD conditions on the charge transport dynamics (i.e., D_{ct} values), we used a redox thin film model[36,42–44] (Section S6, Supporting Information) to simulate the instantaneous current responses of PVF during linear potential sweeping at varying scan rates (ν_s) using a series of different D_{ct} values. Figure 2h shows a heat map of simulated ΔE_p–ν_s data with varying β, which is defined as the ratio of the D_{ct} value for pure PVF to the reduced D_{ct} value for PVF with a hydrogel coating (i.e., $\beta = D_{ct}^{PVF}/D_{ct}^{PVF\text{-}h}$). On overlaying of the experimentally obtained ΔE_p–ν_s data over the simulated heat map, we observed that, compared to untreated PVF, short iCVD treatments (0.5–3 h) decreased D_{ct} by ≈20-fold (i.e., $\beta \approx 20$), while a longer treatment (4.5 h) reduced D_{ct} by ≈50-fold.

Galvanostatic (GV) cycling (Figure S2a, Supporting Information) yielded conclusions consistent with the CV measurements (Figure 2e): the capacity retention after 10 000 GV cycles at 1.34 A g^{-1} was 58% for PVF/CP without PHEMAx, whereas the capacity retention after 10 000 GV cycles at 1.23 A g^{-1} was nearly 100% for PVF-h/CP with a 3 h iCVD treatment. Electrochemical impedance spectroscopic (EIS) measurements (Figure S2b, Supporting Information) show that the combined series resistances (R_s) for PVF-h/CP with 0.5, 1.5, and 3 h treatments were 35.9, 36.2, and 37.4 Ω, respectively, close to the value for untreated PVF (35.7 Ω), whereas the 4.5 h treatment resulted in a larger R_s value (54.1 Ω).

Next, we investigated the applicability of our soft confinement approach for stabilizing EAPs beyond PVF. EAPs are categorized into two general classes: redox polymers with unconjugated backbones and intrinsically conducting polymers (ICPs) with conjugated backbones.[19,41] The PVF films studied earlier belong to the first category. ICPs are also widely used in electrochemical applications and their performance stability is an even more severe issue than that of redox polymers because the rigid conjugated backbones make ICPs more prone to electrochemical degradation during cyclic operation.[19] Hence, it was of interest to study whether our stabilization approach would be effective for ICPs. We used polypyrrole (PPY) as the model ICP system, which has been employed widely as the active component in energy storage devices.[18] We first studied the impact of incorporation of PHEMAx on the cycling stability of PPY electrochemically deposited on CP. SEM images of PPY/CP and PPY-h/CP (3 h iCVD treatment) (**Figure 3**a,b) show clear morphological differences, indicating conformal coating of PHEMAx on top of PPY. XPS survey scans (Figure 3c) demonstrate that after the iCVD treatment, the N_{1s} peak disappears, confirming a complete coverage of the PPY layer by PHEMAx around the PPY-h/CP fibers. CV tests at 0.1 V s^{-1} reveal that PPY-h/CP had significantly improved cycling stability, with 98% capacity retention compared to only 17% retention for PPY/CP (Figure 3d). Notably, the PPY films deposited on CP exhibits a nonporous structure (see Figure 3a). Nanostructured ICPs possessing increased surface area and shortened ion diffusion pathways usually exhibit higher capacitances than do their nonporous counterparts; however, nanosized ICPs usually have more brittle structures, and therefore further deteriorated cycling stability.[14,20] To investigate whether the PHEMAx coating can also improve cycling stability of nanostructured ICPs, we prepared free-standing nanostructured PPY gels (nPPY; Figure 3e inset shows photographs of free-standing pellet-like nPPY gels). SEM imaging shows that the as-prepared nPPY exhibits a porous structure comprised of spherical particles (Figure 3e). After the iCVD treatment, the particles present a more rounded morphology, indicating the existence of a PHEMAx coating (Figure 3f). The coating displays a high degree of conformality, showing practically no blockage of the pores, which is crucial for preserving the desired advantages of the porous nanostructures. The absence of a N_{1s} peak and the O/C ratio being consistent with that of HEMA in the XPS spectrum of nPPY-h (Figure 3g) confirms that the interfaces in nPPY-h are completely covered by PHEMAx. Compared to

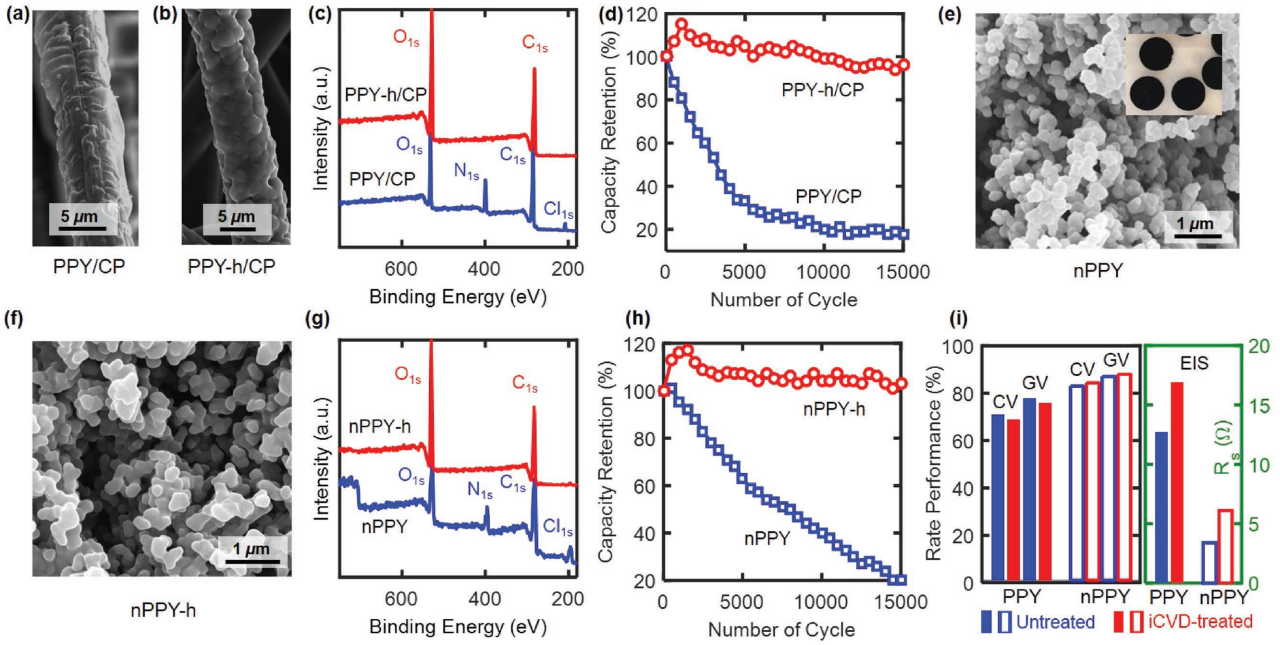

Figure 3. Representative SEM images of a) PPY/CP and b) PPY-h/CP. c) XPS spectra of PPY/CP and PPY-h/CP. d) Capacity retention versus number of CV cycles for PPY/CP and PPY-h/CP. CV was performed at 0.1 V s^{-1} in 0.5 M $NaClO_4$ using a three-electrode configuration. e) Representative SEM image of nPPY. Inset: photographs of free-standing nPPY pellets with a diameter of ≈9 mm. f) Representative SEM image of nPPY-h. g) XPS spectra of nPPY and nPPY-h. h) Capacity retention versus number of CV cycles for nPPY and nPPY-h. CV was performed at 0.1 V s^{-1} in 0.5 M $NaClO_4$ using a three-electrode configuration. i) Summary of rate performance (left panel, measured by CV and GV) and R_s values (right panel, measured by EIS) for PPY and nPPY without (blue bars) and with iCVD treatment (red bars). Rate performance measured by CV or GV measurements was defined as the ratio between the specific capacitance obtained at 0.2 V s^{-1} or ≈5 A g^{-1} and that obtained at 0.01 V s^{-1} or ≈1 A g^{-1}. The PHEMAx coatings of PPY-h/CP and nPPY-h were prepared by a 3 h iCVD treatment.

nPPY, nPPY-h displays substantially improved cycling stability (Figure 3h). Importantly, for both the PPY and nPPY cases, we did not observe significantly compromised transport rates or increased resistances due to the iCVD treatment, as shown in Figure 3i, which summarizes the capacitance decay with increased operation rate (scan rate for CV or current density for GV), and the R_s values obtained from EIS. Plots of capacitance versus scan rate or current density, and EIS spectra are shown in Figure S5 (Supporting Information).

To confirm that the PHEMAx coating can mitigate the structural pulverization and/or detachment from the substrates, we investigated the morphologies of PHEMAx-coated EAPs and unmodified EAPs after electrochemical cycling experiments. The SEM images of PVF/CP, PVF-h/CP, PPY/CP, and PPY-h/CP before and after 10 000 CV cycles at 0.1 V s^{-1} are shown in Figure S6 (Supporting Information). It can be seen clearly that after cycling experiments, the EAPs without PHEMAx underwent significant morphological variation and/or detached from the CP substrate, whereas PHEMAx-coated EAPs maintained structural integrity.

Recently, a demand for improving the mechanical stability of EAP systems under strained conditions has emerged for the development of flexible, bendable electronics.[8,16] To show that the soft confinement approach is applicable for improving the mechanical stability of EAPs under strained conditions, we conducted bending and twisting tests for PHEMAx-coated PVF and PPY (representing redox polymers and ICPs, respectively) integrated into a flexible carbon cloth (CC) substrate. A bending cycle is defined as the compressive flexing of the electrode with a mechanical tester over a range of angles from 180° to 100° (radius = 3 mm) and then a return of the electrode to its original position (**Figure 4**a). The thickness of the electrode was ≈0.4 mm, estimated from the SEM cross-sectional analysis (Figure S7a, Supporting Information), so the maximum strain during bending was 6.7% (for calculation details, see Figure S7b in the Supporting Information). Figure 4b shows the capacitance retention versus number of bending cycles for PVF/CC, PVF-h/CC, PPY/CC, and PPY-h/CC. Without the hydrogel coating, PVF/CC showed only 59.3% capacity retention after 3000 bending cycles, possibly due to the expected stress-induced detachment of polymer films from CC yarns under strained conditions. In contrast, PVF-h/CC showed remarkably improved capacity retention (90.8%) after the same number of bending cycles, demonstrating that the robust soft confinement reduced the degree of EAP detachment. Similar results were observed for PPY-based systems: after 2500 bending cycles, PPY/CC retained only 41.7% of its initial specific capacity, whereas PPY-h/CC preserved 93.1% of its initial specific capacity. We further performed twisting tests, whereby each twisting cycle is defined as the rotation of a 1 cm × 16 cm electrode by 360° × 8 = 2880° with a controlled electrical drill followed by a return to its original position (Figure 4c). The twisted electrode took on a cylinder-like shape with an average diameter of ≈4.5 cm, consistent with a maximum strain of 8.9% during twisting (for calculation details, see Figure S7c in the Supporting Information). The capacity retentions of

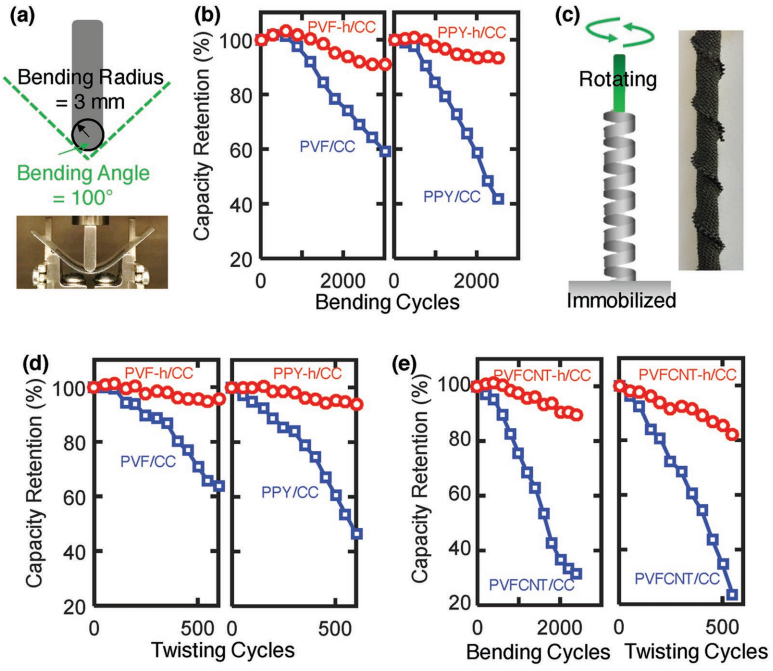

Figure 4. a) Schematic illustration of the bending test condition. Photograph shows an example of a bent electrode. b) Capacity retention versus number of bending cycles for PVF/CC, PVF-h/CC, PPY/CC, and PPY-h/CC. Specific capacities were measured by CV at 0.15 V s^{-1} in 0.5 M $NaClO_4$ using a three-electrode configuration. c) Schematic illustration of the twisting test conditions. Photograph shows an example of a twisted electrode. d) Capacity retention versus number of twisting cycles for PVF/CC, PVF-h/CC, PPY/CC, and PPY-h/CC. Specific capacities were measured by CV at 0.15 V s^{-1} in 0.5 M $NaClO_4$ using a three-electrode configuration. e) Capacity retention versus number of bending or twisting cycles for PVFCNT/CC and PVFCNT-h/CC.

PVF/CC, PVF-h/CC, PPY/CC, and PPY-h/CC after 600 such twisting cycles (Figure 4d) were calculated to be 63.6%, 95.7%, 46.7%, and 93.7%, respectively, demonstrating that the samples with the hydrogel coating exhibited a stronger preservation of their energy storage performance under twisting conditions. Composite materials containing EAP and "nanofillers" such as carbon nanotubes and activated carbon usually display high energy densities and excellent rate performance.[14,20] These materials are, however, more susceptible to mechanical stress since these "nanofillers" fall off their substrates easily.[45] Therefore, we moved on to investigate if our EAP stabilization approach would be effective for EAP/nanofiller composites. We modified CC substrates with nanocomposites consisting of PVF and metallic carbon nanotubes (CNTs) by electrochemical deposition from stable suspensions containing PVFCNT complexes formed via the strong π-stacking interaction between the cyclopentadiene rings of PVF and the sp^2-carbon surfaces of CNTs.[46] The resulting PVFCNT nanocomposites (polymer to CNT mass ratio ≈ 4) typically exhibited pores with an average diameter of ≈50–100 nm and Brunauer–Emmett–Teller (BET) surface area of 112 m^2 g^{-1}.[46] Compared to PVF/CC and PPY/CC, PVFCNT showed poorer performance stability under strained conditions (Figure 4e): the capacity retention of PVFCNT/CC was 31.6% after 2400 bending cycles and 23.5% after 550 twisting cycles. Remarkably, the encapsulation of PVFCNT nanocomposites with a hydrogel coating led to significantly improved performance stability: the capacity retentions for PVFCNT-h/CC after the same bending and twisting tests as for PVFCNT/CC were 89.7% and 82.1%, respectively.

To demonstrate the effectiveness of the soft confinement strategy in practical energy storage devices, we constructed a flexible solid-state asymmetrical supercapacitor (ASC) and studied the influence of the PHEMAx coating on its performance stability. ASC modified with PHEMAx is denoted as ASC-h. The ASC (**Figure 5**a) consisted of PVFCNT as the positive electrode and poly(3,4-ethylenedioxythiophene) (PEDOT) synthesized by oxidative chemical vapor deposition as the negative electrode. The asymmetrical configuration was adopted to enhance the energy densities by providing matching operating potential ranges between the positive and negative electrodes (Section S7, Supporting Information). As controls, we prepared symmetric PVFCNT and PEDOT supercapacitors. CV profiles (Figure 5b) show that the asymmetrical devices yielded significantly higher current densities than those obtained with the symmetric devices. Notably, the asymmetric devices exhibited the desired redox peaks of ferrocene, whereas the symmetric devices failed to produce such redox peaks. For comparison, CVs of PEDOT and PVFCNT in a three-electrode configuration are shown in Figure 5c,d, respectively. The Ragone plot (Figure 5e) shows that ASC and ASC-h achieved maximum energy densities of 32.4 and 31.2 Wh kg^{-1}, respectively, significantly larger than the values for symmetrical devices with either PEDOT (3.37 Wh kg^{-1}) or PVFCNT (6.26 Wh kg^{-1}). The capacitance retentions of ASC and ASC-h after 10 000 GV charging/discharging cycles, 4000 bending cycles, and 800 twisting cycles (rotation span = 360° × 1/2 = 180°) are summarized in Figure 5f, based on which it is evident that incorporation of PHEMAx improved the performance stability significantly. The capacitance retentions versus the number of GV cycles, bending cycles, and twisting cycles are shown in Figure S8a–c (Supporting Information), respectively.

3. Conclusion

In conclusion, we have developed a "soft confinement" approach to improving EAP performance stability by using iCVD-synthesized PHEMAx films that, when in contact with electrolyte solutions, become hydrogel coatings encapsulating the EAP microstructures. Fundamentally distinct from commonly used "scaffolding" or "synthetic" approaches, our strategy enjoys the unique advantage of substrate-independency, and hence is broadly applicable to EAPs of different chemical characteristics and morphologies. We have demonstrated that our strategy led to remarkably enhanced

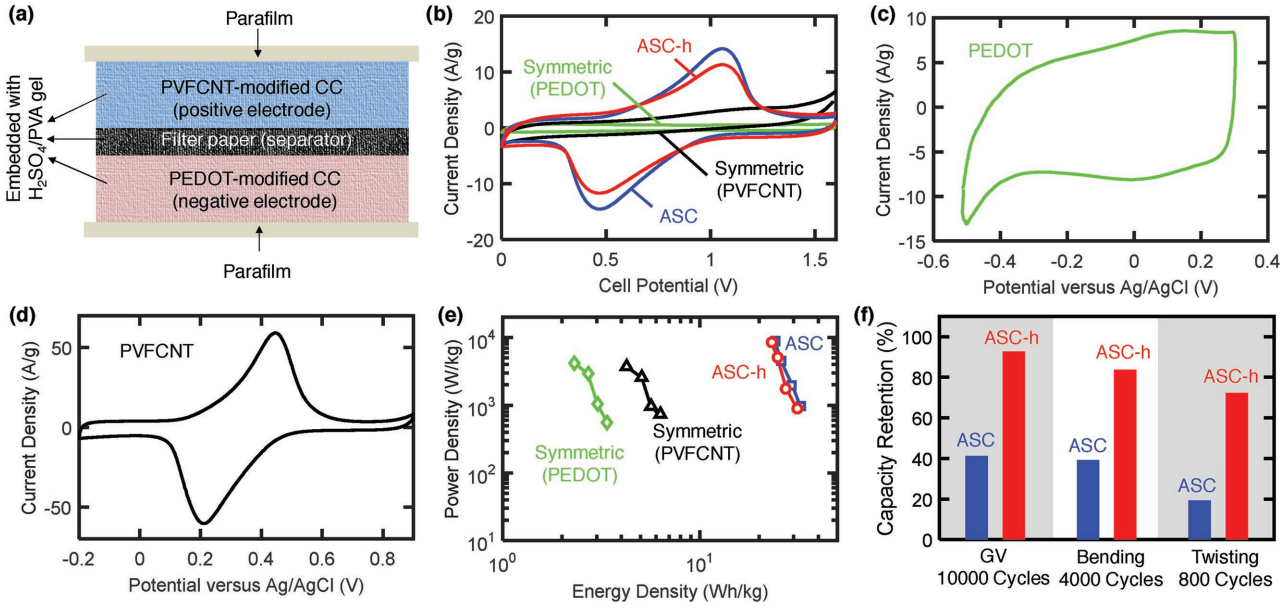

Figure 5. a) Schematic illustration of the flexible solid-state asymmetric supercapacitor that consists of a PVFCNT-h positive electrode and a PEDOT-h negative electrode. b) CV curves (0.05 V s^{-1}) obtained with a symmetric PEDOT supercapacitor, symmetric PVFCNT supercapacitor, ASC, and ASC-h. c) CV curve of a PEDOT electrode obtained in 1 M H_2SO_4 at a scan rate of 0.05 V s^{-1} with a three-electrode configuration. d) CV curve of a PVFCNT electrode obtained in 1 M H_2SO_4 at a scan rate of 0.05 V s^{-1} with a three-electrode configuration. e) Ragone plots for the symmetric PEDOT, PVFCNT supercapacitors, ASC, and ASC-h. f) Comparison of capacity retention between ASC and ASC-h when subjected to 10 000 GV cycles, 4000 bending cycles, and 800 twisting cycles. GV measurements were performed at 1.2 A g^{-1} for ASC and 1.4 A g^{-1} for ASC-h. For bending and twisting tests, the specific capacities were determined by CV measurements at 0.1 V s^{-1}. The PHEMAx coatings of PVF-h/CC, PPY-h/CC, PVFCNT-h/CC, and ASC-h were prepared by a 3 h iCVD treatment.

performance stabilities of different types of EAP systems, under various testing conditions, including repeated charging/discharging, bending, and twisting. We anticipate that our soft confinement approach could also be used in combination with other EAP stabilization methods, taking the performance stability of EAPs to a higher level. Furthermore, our strategy could be extended to many other EAP applications beyond energy storage, where the stabilization and reusability of EAPs are crucial for realizing practical long-term operations. Such applications may include EAP-based electrochemically mediated sensing, catalysis, and separations, since the hydrogel coatings can be rationally engineered by modulating iCVD precursors and conditions for tunable chemical compositions and mesh sizes. The engineered coating could accommodate the key species that interact with the EAPs for these applications, such as target biomolecules to be detected for sensing purposes, reactants of interest in catalytic cycles, or pollutants to be removed in separation processes.

4. Experimental Section

Materials: PVF (molecular weight = 50 000 g mol^{-1}) was obtained from Polysciences. Pyrrole, sodium perchlorate, tetrabutylammonium perchlorate, chloroform, ethanol, sulfuric acid, *tert*-butyl peroxide (TBPO) (98%), HEMA (≥ 99%), DEGDVE (99%), EDOT (97%), polyvinyl alcohol (PVA, molecular weight = 61 000 g mol^{-1}), 2,2-dimethoxy-2-phenylacetophenone (99%, Aldrich), multiwalled carbon nanotubes (MWCNTs) with a diameter of 6–9 nm and purity of 95% were obtained from Sigma-Aldrich. A platinum wire auxiliary electrode and an Ag/AgCl (3 M NaCl) reference electrode were purchased from BASi. All reagents were used as received throughout the study, without further purification or chemical modification unless otherwise noted.

Synthesis of EAP Systems: The typical procedure used to perform electrochemical deposition of EAPs onto carbon substrates is as follows. The PVF/CP or PVF/CC electrode system was prepared by applying a potential of 0.8 V versus Ag/AgCl to the CP or CC substrate with a nominal surface area of 1 cm^2 for 10 min in 5 mL chloroform solution containing 10 mg mL^{-1} PVF and 0.1 M tetrabutylammonium perchlorate. The affinity of ferrocene moieties in PVF for hydrophobic organic solvents (e.g., chloroform) is reduced upon oxidation. Therefore, PVF initially soluble in chloroform became solvophobic and subsequently precipitated onto the fiber when it was oxidized at the fiber surface. The PPY/CP or PPY/CC electrode system was prepared by electrochemical polymerization of pyrrole through application of a potential of 0.6 V versus Ag/AgCl to the CP or CC substrate for 5 min in 5 mL water containing 0.1 M pyrrole and 0.1 M sodium perchlorate. The PVFCNT/CC electrode system was prepared by repeating the following electrochemical deposition for several times: application of a potential of 0.8 V versus Ag/AgCl to the CC substrate with a nominal surface area of 1 cm^2 for 2 min in 5 mL chloroform solution containing 10 mg mL^{-1} PVF, 2 mg mL^{-1} MWCNTs, and 0.1 M tetrabutylammonium perchlorate. Typically, the deposition process was repeated for three to four times, and between each deposition, cyclic voltammetric measurements were performed to track the quantity of PVF deposited. It is to be noted that MWCNTs and PVF formed stable suspensions in chloroform after sonication for 45 min.[46] In a typical synthesis of nanostructured PPY hydrogels, 6.3 mmol pyrrole was dissolved in 3 mL water/ethanol (v/v 1:1) mixed solvent (solution A). Solution B was prepared by dissolving 6.3 mmol $FeCl_3$ and 6.3 mmol $NaNO_3$ in 3 mL water. Next, solution A and solution B were cooled to 0–4 °C, and then mixed under vigorous agitation. The mixture was stored at room temperature for 30 d and the resulting PPY hydrogel was purified by immersion in a water/ethanol mixed solvent under stirring for 24 h. Finally, the dehydrated PPY hydrogel was obtained by allowed to dry in a vacuum oven at 60 °C for 48 h.

Synthesis of PHEMAx by iCVD: The iCVD process and its reactor configuration have been described in detail elsewhere.[47] PHEMAx was synthesized and simultaneously deposited onto porous EAP electrodes via iCVD. A silicon wafer was also placed in the reactor to harvest iCVD-deposited polymer, for the purpose of in situ thickness monitoring and polymer characterization. The monomer HEMA (heated at 75 °C) was delivered in the vapor phase introduced to the iCVD reactor at 0.45 sccm, together with the cross-linker DEGDVE (heated at 60 °C) at 0.3 sccm. The vapor of initiator TBPO was metered at 1.0 sccm. The reactor pressure was controlled at 300 mTorr by a throttle valve. The stage temperature was back-cooled and maintained at 40 °C. The filament temperature was heated resistively at 250 °C. For PVF/CP electrodes, four treatment times (0.5, 1.5, 3, and 4.5 h) were investigated. For all other electrodes, 3 h of iCVD treatment was used.

Fabrication of the Solid-State Flexible Supercapacitor: The solid-state supercapacitor (symmetric or asymmetric) was assembled by two pieces of EAP-integrated CC electrodes on either side of a separator (VWR Grade 415 Filter Paper) with a H_2SO_4/PVA gel as the solid electrolyte. The H_2SO_4/PVA gel was prepared by mixing concentrated sulfuric acid, PVA, and deionized water (mass ratio = 1:1:10) and heating at 90 °C under stirring for 1 h. The two electrodes and separator were soaked in the hot gel for about 5 min and then assembled together. The as-prepared device was kept in an oven at 65 °C for 24 h to remove excess water in the electrolyte, and then sealed with Parafilm to prevent water absorption.

Supporting Information

Supporting Information is available from the Wiley Online Library or from the author.

Acknowledgements

X.M. and A.L. contributed equally to this work. The authors thank Dr. Jose Yagüe at the Institut Quimic de Sarria for his generous help with mesh size calculation. Hongmou Zhang from the Department of Urban Studies and Planning at the Massachusetts Institute of Technology is acknowledged for help with the visuals.

Conflict of Interest

The authors declare no conflict of interest.

Keywords

chemical vapor deposition, electrochemically active polymers, energy storage, flexible devices, performance stability

Received: November 6, 2017
Published online: January 8, 2018

[1] J. Kim, J. Lee, J. You, M. S. Park, M. S. Al Hossain, Y. Yamauchi, J. H. Kim, *Mater. Horiz.* **2016**, *3*, 517.
[2] S. Holliday, R. S. Ashraf, A. Wadsworth, D. Baran, S. A. Yousaf, C. B. Nielsen, C.-H. Tan, S. D. Dimitrov, Z. Shang, N. Gasparini, M. Alamoudi, F. Laquai, C. J. Brabec, A. Salleo, J. R. Durrant, I. McCulloch, *Nat. Commun.* **2016**, *7*, 11585.
[3] B. Russ, A. Glaudell, J. J. Urban, M. L. Chabinyc, R. A. Segalman, *Nat. Rev. Mater.* **2016**, *1*, 16050.
[4] A. Liu, P. Kovacik, N. Peard, W. Tian, H. Goktas, J. Lau, B. Dunn, K. K. Gleason, *Adv. Mater.* **2017**, *29*, 1606091.
[5] D. Svirskis, J. Travas-Sejdic, A. Rodgers, S. Garg, *J. Controlled Release* **2010**, *146*, 6.
[6] R. Feiner, L. Engel, S. Fleischer, M. Malki, I. Gal, A. Shapira, Y. Shacham-Diamand, T. Dvir, *Nat. Mater.* **2016**, *15*, 679.
[7] J. Y. Oh, S. Rondeau-Gagne, Y. C. Chiu, A. Chortos, F. Lissel, G. J. N. Wang, B. C. Schroeder, T. Kurosawa, J. Lopez, T. Katsumata, J. Xu, C. X. Zhu, X. D. Gu, W. G. Bae, Y. Kim, L. H. Jin, J. W. Chung, J. B. H. Tok, Z. N. Bao, *Nature* **2016**, *539*, 411.
[8] T. Someya, Z. N. Bao, G. G. Malliaras, *Nature* **2016**, *540*, 379.
[9] R. Green, M. R. Abidian, *Adv. Mater.* **2015**, *27*, 7620.
[10] W. B. Guo, X. D. Zhang, X. Yu, S. Wang, J. C. Qiu, W. Tang, L. L. Li, H. Liu, Z. L. Wang, *ACS Nano* **2016**, *10*, 5086.
[11] X. Su, K.-J. Tan, J. Elbert, C. Ruttiger, M. Gallei, T. F. Jamison, T. A. Hatton, *Energy Environ. Sci.* **2017**, *10*, 1272.
[12] X. Su, H. J. Kulik, T. F. Jamison, T. A. Hatton, *Adv. Funct. Mater.* **2016**, *26*, 3394.
[13] D. S. Achilleos, T. A. Hatton, *ACS Appl. Mater. Interfaces* **2016**, *8*, 32743.
[14] Y. Shi, L. L. Peng, Y. Ding, Y. Zhao, G. H. Yu, *Chem. Soc. Rev.* **2015**, *44*, 6684.
[15] C. O. Baker, X. Huang, W. Nelson, R. B. Kaner, *Chem. Soc. Rev.* **2017**, *46*, 1510.
[16] B. C. Kim, J.-Y. Hong, G. G. Wallace, H. S. Park, *Adv. Energy Mater.* **2015**, *5*, 1500959.
[17] T. Y. Liu, L. Finn, M. H. Yu, H. Y. Wang, T. Zhai, X. H. Lu, Y. X. Tong, Y. Li, *Nano Lett.* **2014**, *14*, 2522.
[18] Y. Song, T. Y. Liu, X. X. Xu, D. Y. Feng, Y. Li, X. X. Liu, *Adv. Funct. Mater.* **2015**, *25*, 4626.
[19] G. Inzelt, in *Conducting Polymers: A New Era in Electrochemistry* (Ed: F. Scholz), Springer, Berlin, **2012**, pp. 83–147.
[20] S. Ghosh, T. Maiyalagan, R. N. Basu, *Nanoscale* **2016**, *8*, 6921.
[21] X. H. Xia, D. L. Chao, Z. X. Fan, C. Guan, X. H. Cao, H. Zhang, H. J. Fan, *Nano Lett.* **2014**, *14*, 1651.
[22] W. Q. Zhao, S. S. Wang, C. H. Wang, S. T. Wu, W. J. Xu, M. C. Zou, A. Ouyang, A. Y. Cao, Y. B. Li, *Nanoscale* **2016**, *8*, 626.
[23] C. Zhou, Y. W. Zhang, Y. Y. Li, J. P. Liu, *Nano Lett.* **2013**, *13*, 2078.
[24] W. Li, F. Gao, X. Wang, N. Zhang, M. Ma, *Angew. Chem., Int. Ed.* **2016**, *55*, 9196.
[25] D. F. Zeigler, S. L. Candelaria, K. A. Mazzio, T. R. Martin, E. Uchaker, S. L. Suraru, L. J. Kang, G. Z. Cao, C. K. Luscombe, *Macromolecules* **2015**, *48*, 5196.
[26] G.-F. Chen, X.-X. Li, L.-Y. Zhang, N. Li, T. Y. Ma, Z.-Q. Liu, *Adv. Mater.* **2016**, *28*, 7680.
[27] D. Vonlanthen, P. Lazarev, K. A. See, F. Wudl, A. J. Heeger, *Adv. Mater.* **2014**, *26*, 5095.
[28] F. Carpi, D. De Rossi, R. Kornbluh, R. E. Pelrine, P. Sommer-Larsen, *Dielectric Elastomers as Electromechanical Transducers: Fundamentals, Materials, Devices, Models and Applications of an Emerging Electroactive Polymer Technology*, Elsevier, Amsterdam **2008**.
[29] A. Asatekin, K. K. Gleason, *Nano Lett.* **2011**, *11*, 677.
[30] M. Wang, X. Wang, P. Moni, A. Liu, D. H. Kim, W. J. Jo, H. Sojoudi, K. K. Gleason, *Adv. Mater.* **2017**, *29*, 1604606.
[31] A. M. Coclite, R. M. Howden, D. C. Borrelli, C. D. Petruczok, R. Yang, J. L. Yagüe, A. Ugur, N. Chen, S. Lee, W. J. Jo, A. Liu, X. Wang, K. K. Gleason, *Adv. Mater.* **2013**, *25*, 5392.
[32] K. Chan, K. K. Gleason, *Langmuir* **2005**, *21*, 8930.
[33] W. D. Tian, X. W. Mao, P. Brown, G. C. Rutledge, T. A. Hatton, *Adv. Funct. Mater.* **2015**, *25*, 4803.
[34] X. Mao, E. H. Yan, G. C. Rutledge, T. A. Hatton, *Chem. Mater.* **2016**, *28*, 543.

[35] R. Pietschnig, *Chem. Soc. Rev.* **2016**, *45*, 5216.
[36] X. Mao, W. Tian, J. Wu, G. C. Rutledge, T. A. Hatton, *J. Am. Chem. Soc.* **2015**, *137*, 1348.
[37] J. L. Yague, K. K. Gleason, *Soft Matter* **2012**, *8*, 2890.
[38] C. Zhong, Y. Deng, W. Hu, J. Qiao, L. Zhang, J. Zhang, *Chem. Soc. Rev.* **2015**, *44*, 7484.
[39] J. M. Cooper, R. Cubitt, R. M. Dalgliesh, N. Gadegaard, A. Glidle, A. R. Hillman, R. J. Mortimer, K. S. Ryder, E. L. Smith, *J. Am. Chem. Soc.* **2004**, *126*, 15362.
[40] M. E. G. Lyons, in *Advances in Chemical Physics* (Eds: I. Prigogine, S. A. Rice), John Wiley & Sons, Inc., Hoboken, NJ, USA **1996**, pp. 297–624.
[41] C. Gabrielli, H. Perrot, in *Modern Aspects of Electrochemistry No. 44: Modelling and Numerical Simulations II* (Ed: M. Schlesinger), Springer, New York, NY **2009**, pp. 151–238.
[42] A. J. Bard, L. R. Faulkner, *Electrochemical Methods: Fundamentals and Applications*, 2nd ed., John Wiley & Sons, Inc., New York, NY **2001**.
[43] A. Merz, A. J. Bard, *J. Am. Chem. Soc.* **1978**, *100*, 3222.
[44] P. J. Peerce, A. J. Bard, *J. Electroanal. Chem. Interfacial Electrochem.* **1980**, *114*, 89.
[45] X. Zhang, L. Wang, J. Peng, P. Cao, X. Cai, J. Li, M. Zhai, *Adv. Mater. Interfaces* **2015**, *2*, 1500267.
[46] X. Mao, G. C. Rutledge, T. A. Hatton, *Langmuir* **2013**, *29*, 9626.
[47] K. K. S. Lau, K. K. Gleason, *Macromolecules* **2006**, *39*, 3688.